ACS APPLIED MATERIALS & INTERFACES

Research Article

www.acsami.org

Sulfonic Acid- and Lithium Sulfonate-Grafted Poly(Vinylidene Fluoride) Electrospun Mats As Ionic Liquid Host for Electrochromic Device and Lithium-Ion Battery

Rui Zhou,[†] Wanshuang Liu,[†] Yew Wei Leong,[‡] Jianwei Xu,[‡] and Xuehong Lu*[,†]

[†]School of Materials Science and Engineering, Nanyang Technological University, 50 Nanyang Avenue, Singapore, 639798

[‡]Institute of Materials Research & Engineering, 3 Research Link, Singapore, 117602

Supporting Information

ABSTRACT: Electrospun polymer nanofibrous mats loaded with ionic liquids (ILs) are promising nonvolatile electrolytes with high ionic conductivity. The large cations of ILs are, however, difficult to diffuse into solid electrodes, making them unappealing for application in some electrochemical devices. To address this issue, a new strategy is used to introduce proton conduction into an IL-based electrolyte. Poly(vinylidene fluoride-co-hexafluoropropylene) (P(VDF-HFP)) copolymer is functionalized with sulfonic acid through covalent attachment of taurine. The sulfonic acid-grafted P(VDF-HFP) electrospun mats consist of interconnected nanofibers, leading to remarkable improvement in dimensional stability of the mats. IL-based polymer electrolytes are prepared by immersing the modified mats in 1-butyl-3-methylimidazolium tetrafluoroborate ($BMIM^+BF_4^-$). It is found that the SO_3^- groups can have Lewis acid−base interactions with the cations ($BMIM^+$) of IL to promote the dissociation of ILs, and provide additional proton conduction, resulting in significantly improved ionic conductivity. Using this novel electrolyte, polyaniline-based electrochromic devices show higher transmittance contrast and faster switching behavior. Furthermore, the sulfonic acid-grafted P(VDF-HFP) electrospun mats can also be lithiated, giving additional lithium ion conduction for the IL-based electrolyte, with which $Li/LiCoO_2$ batteries display enhanced C-rate performance.

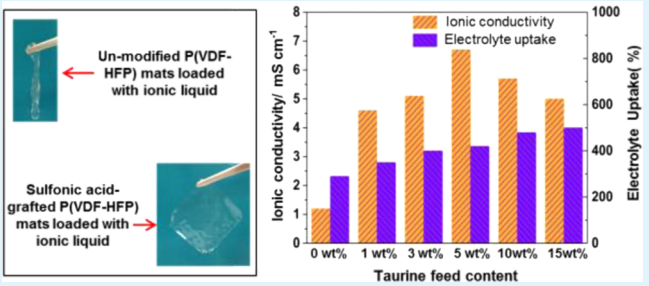

KEYWORDS: *ionic liquid, electrolyte, sulfonic acid, electrochromic device, lithium-ion battery*

1. INTRODUCTION

Polymer electrolytes play indispensable role as ionic conductor in various electrochemical devices, including fuel cells, lithium-ion batteries, supercapacitors and electrochromic devices.[1−5] Enormous efforts have therefore been devoted to develop novel electrolytes for efficient ion transport. Room-temperature ionic liquids, a class of materials composing entirely of ions and having melting points less than 25 °C, have received intense attention.[6−12] The attractiveness of the ionic liquids (ILs) for the use in electrolytes lies upon their nonflammability and nonvolatility as well as excellent electrochemical and thermal stability. These unique features of the ILs render them promising substitutes for traditional liquid electrolytes, which typically contain toxic and flammable solvents. To prepare IL-based electrolyte, a polymer host has to be used to immobilize the ILs.[13] Many polymers have been investigated for hosting the ILs, among which poly(vinylidene fluoride) (PVDF) and its copolymers are especially preferred because of their high dielectric constant, low cost and good stabilities.[14] Recently, the incorporation of ILs into electrospun PVDF mats has emerged as a promising approach to improve the performance of electrochemical devices.[2,9,15,16] The interpenetrating pores in the electrospun mats facilitate the movement of ions, giving rise to high ionic conductivity of the resultant electrolytes.[15,17]

Although ILs can serve as ion sources in electrolytes, the large ion sizes of the ILs cause difficulties for the ions to diffuse into solid working electrodes, making them unappealing for many electrochemical devices. Strategies have been proposed to overcome the aforementioned limitation by introducing smaller ions, such as lithium ions (Li^+), into the IL phase.[18,19] An increase in Li^+ transport property is, however, usually accompanied by a decrease of ionic conductivity. It is because each Li^+ cations can coordinate with multiple anions, forming negatively charged complexes and hence resulting in a higher viscosity and lower conductivity.[20−22] An alternative approach is to graft proton carriers onto PVDF polymer chains, forming proton-conducting IL host. Especially, sulfonic acid-grafted PVDF membranes have been extensively explored as potential proton conducting materials. It is commonly prepared by grafting styrene or substituted styrene monomers onto

Received: May 10, 2015
Accepted: July 13, 2015
Published: July 13, 2015

ACS Publications © 2015 American Chemical Society

DOI: 10.1021/acsami.5b04034
ACS Appl. Mater. Interfaces 2015, 7, 16548−16557

fluorinated polymer chains via electron beam radiation followed by sulfonation reactions.[23−25]

Taurine is a sulfur-containing amino acid ubiquitously distributed in animal tissues[26] and can be chemically synthesized at low cost. Due to the strong polarity of C−F bond, amines are well-known effective reagents for the introduction of functional groups onto fluoropolymer main chains.[27−29] In this work, taurine was directly grafted onto poly(vinylidene fluoride-co-hexafluoropropylene) (P(VDF-HFP)) polymer chains through a reaction in solution. This not only simplifies preparation procedures but also makes the process more economically viable. The obtained sulfonic acid-grafted P(VDF-HFP) was then electrospun, and used as the host for a commonly used IL, 1-butyl-3-methylimidazolium tetrafluoroborate ($BMIM^+BF_4^-$). Herein we report that the sulfonic acid-grafted P(VDF-HFP) electrospun mats have network structure owing to the branching and merging of the nanofibers, leading to remarkable improvement in dimensional stability of the mats. In addition, the sulfonic acid groups attached on the polymer chains can serve as proton sources, contributes significantly to proton conduction. Meanwhile, the negatively charged SO_3^- groups also coordinate with the cations, promoting the dissociation of the IL. Both effects benefit the ion conduction properties of the electrolytes. When they are used as the solvent-free electrolytes in organic electrochromic devices, the devices show excellent electrochromic switching behaviors without the need of incorporation of any small cations such as lithium ions. In addition, the sulfonic acid groups can also be lithiated to form lithium sulfonate-grafted P(VDF-HFP) electrospun mats. When they are used as the host for 1-butyl-1-methylpyrrolidinium bis(trifluoromethylsulfonyl) imide ($PYR_{14}^+TFSI^-$) doped with LiTFSI, the resultant electrolytes show improved lithium transference numbers, and superior C-rate performance in Li/$LiCoO_2$ batteries compared to that of neat P(VDF-HFP) mats.

2. EXPERIMENTAL SECTION

2.1. Materials. Taurine (tauric acid, ≥ 99%), $BMIM^+BF_4^-$ (≥98%), $PYR_{14}^+TFSI^-$ (≥98.5%), LiTFSI (99.95%), sodium hydroxide (NaOH, pellets, semiconductor grade, 99.99%), lithium hydroxide (LiOH, reagent grade, ≥ 98%), magnesium oxide (MgO, 99.99%), aniline (reagent plus grade, 99%), 4-dodecylbenzenesulfonic acid (DBSA, ≥95%), titanium butoxide (reagent grade, 97%), xylene (ACS reagent, ≥ 98.5%), N,N-dimethylformamide (DMF, anhydrous, 99.8%), dimethylacetamide (DMAC, anhydrous, 99.8%), dimethyl ether (≥99%), ethanol (technical grade, 95%) and acetone (analytical reagent grade, 99.98%) were obtained from Sigma-Aldrich Corporation (USA). P(VDF-HFP) powder (solef 11008, M_w = 115,000, molar ratio of VDF/HFP = 9/1) was purchased from Solvay Solexis Inc. (USA). All the chemicals were used without further purification. DBSA-doped polyaniline (PANI)-TiO_2 hybrid was prepared via a sol−gel process involving the reaction of titanium butoxide and a hybrid bridging compound, followed by oxidative emulsion copolymerization of aniline in the presence of the hybrid gel and DBSA.[30] Conducting indium tin oxide (ITO) glass (5−15 Ω $\square^{-1}$) were purchased from Delta Technologies Co. (USA) and cleaned by ultrasonication in a series of solvents including detergent, deionized water, and acetone for 10 min each prior to use.

2.2. Grafting of Sulfonic Acid Group onto P(VDF-HFP) Copolymer. First, tauric acid was transformed to tauric sodium (salt form of taurine) to increase its reactivity with P(VDF-HFP) copolymer. The reaction was performed by dissolving 5.00 g (0.04 mol) of tauric acid in 30 mL of deionized water. Then 1.60 g (0.04 mol) of NaOH was added, and the mixture was stirred at 40 °C for 5 h. The solution was freeze-dried for 72 h to obtain the final product.

Second, tauric sodium was grafted onto P(VDF-HFP) polymer chains. Briefly, 2 g of P(VDF-HFP) and 38 g of DMAC were added in one-necked 100 mL flask with magnetic stirring. After P(VDF-HFP) was fully dissolved in DMAC, desired amounts of tauric sodium and MgO were added, and the mixture was heated and kept at 100 °C for 10 h with vigorous stirring in a nitrogen atmosphere. The weight percentage of taurine with respect to the weight of P(VDF-HFP) were kept at 1, 3, 5, 10, and 15 wt %, respectively, and the molar ratio of tauric sodium/MgO was 2/1. The mixture was then cooled to room temperature, precipitated from dimethyl ether and thoroughly rinsed with deionized water. The sodium sulfonate-grafted P(VDF-HFP) samples were dried at 60 °C under vacuum for 24 h to remove solvent completely.

Finally, the attached $-SO_3Na$ groups were converted to $-SO_3H$. The reaction proceeded by placing the obtained sodium sulfonate-grafted P(VDF-HFP) samples in 2 M HCl solution, and refluxing at 80 °C for 12 h in a nitrogen atmosphere. After thoroughly washing with deionized water, the sulfonic acid-grafted P(VDF-HFP) samples were dried at 60 °C under vacuum.

2.3. Conversion of Sulfonic Acid-Grafted P(VDF-HFP) to Lithium Sulfonate-Grafted P(VDF-HFP). The preparation procedure for lithium sulfonate-grafted P(VDF-HFP) is similar to that for sodium sulfonate-grafted P(VDF-HFP) described above, except that LiOH was used instead of NaOH.

2.4. Electrospinning of Sulfonic Acid- and Lithium Sulfonate-Grafted P(VDF-HFP) Copolymers. A solvent mixture of DMF/acetone was first prepared at the DMF/acetone weight ratio of 60/40, followed by dissolving sulfonic acid-grafted and lithium sulfonate-grafted P(VDF-HFP), respectively, in the solvent mixture at polymer concentration of 18 wt % by mechanical stirring overnight. Electrospinning was conducted at an applied voltage of 18 kV and feeding rate of 0.20 mL/h. The nanofibers were collected on a grounded aluminum foil at a fixed distance of 15 cm from the needle tip. The obtained electrospun mats were vacuum-dried at 60 °C for 12 h before characterization.

2.5. Preparation of IL-Based Polymer Electrolytes. The IL-based polymer electrolytes were obtained by soaking sulfonic acid-grafted P(VDF-HFP) electrospun mats in $BMIM^+BF_4^-$ for 3 h at 60 °C. The IL-swollen electrospun mats were placed onto a piece of cellulose paper and pressed by 20 g weight to absorb excess IL. The electrolyte uptake (ε) was calculated using eq 1

$$\varepsilon\ (\%) = \frac{M - M_0}{M_0} \times 100 \tag{1}$$

where M_0 is the mass of dry electrospun mats and M the mass after soaking with IL electrolytes.

2.6. Characterization. Fourier transform infrared (FTIR) spectra were obtained using attenuated total reflection (ATR) attachment on PerkinElmer instruments Spectrum GX FTIR spectrometer in the transmittance mode with a wavenumber range of 4000−400 cm^{-1}. Nuclear magnetic resonance (^1H NMR) spectra were recorded using a 400 MHz spectrometer in DMSO-d_6. Elemental analysis was performed using a PerkinElmer Instruments CHNS-O Analyzer. Wide angle X-ray diffraction (WAXD) patterns of the electrospun mats were recorded on a Bruker GADDS X-ray diffractometer using Cu Kα radiation (λ = 0.154 nm) generated at 40 kV and 40 mA. Differential scanning calorimetry (DSC) was carried out on Modulated DSC 2010 under nitrogen purge, at a heating rate of 10 °C min^{-1} in the temperature range from −80 to 180 °C. Thermal gravimetric analysis (TGA) was performed on a TA Instruments TGA Q500 (TA Instruments, German) under an air atmosphere over a temperature range of 25−700 °C at a heating rate of 10 °C min^{-1}. The morphologies of the electrospun nanofibrous mats were investigated using a field-emission scanning electron microscope (FESEM, JEOL 7600F). To measure the average diameter of the electrospun mats, 100 fibers in the SEM micrograph were selected randomly and the average value of them was considered as the average fiber diameter. Tensile tests were performed using ITW Instron tester 5567 with a 500 N loaded cell at a crosshead speed of 5 mm min^{-1}. Dog-bone-shaped

DOI: 10.1021/acsami.5b04034
ACS Appl. Mater. Interfaces 2015, 7, 16548−16557

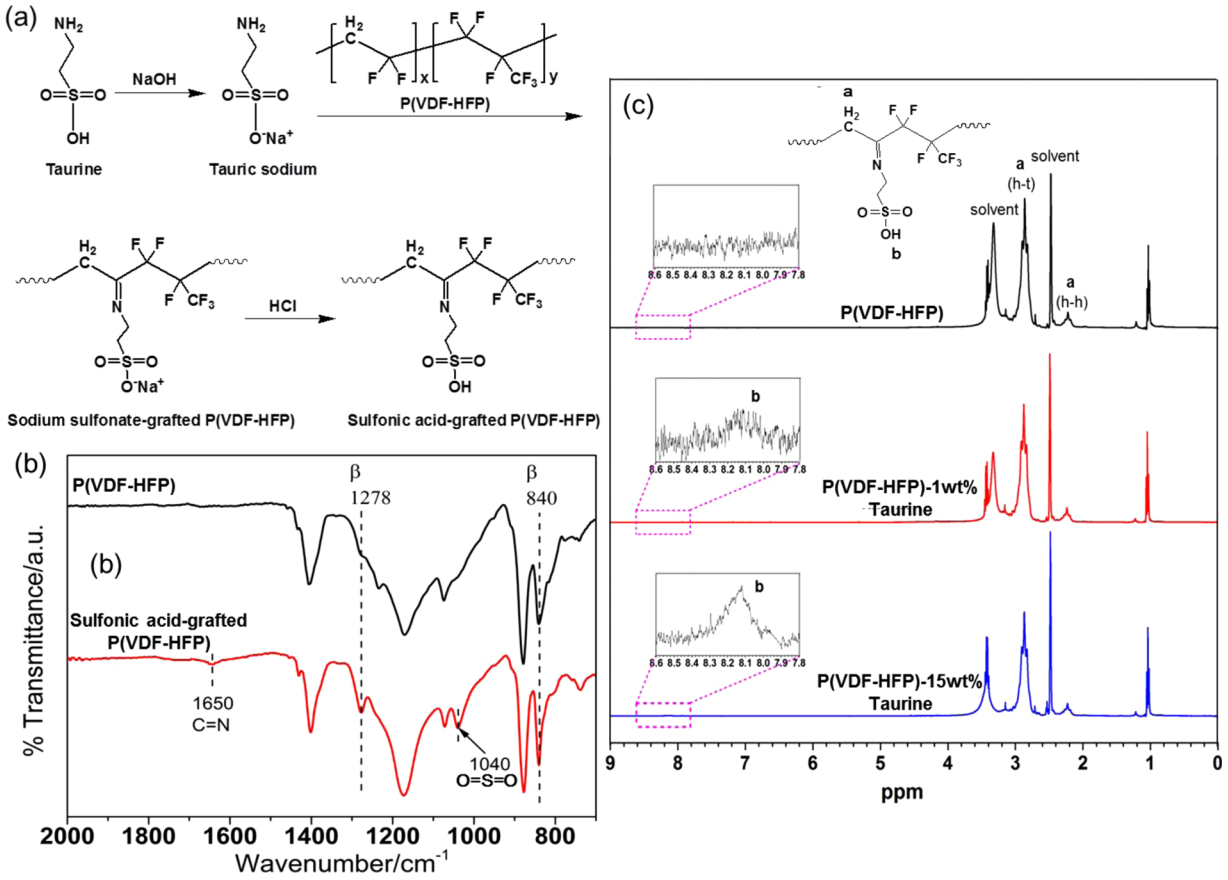

Figure 1. (a) Schematic illustration of synthesis route of sulfonic acid-grafted P(VDF-HFP). (b) FTIR spectra of P(VDF-HFP) and sulfonic acid-grafted P(VDF-HFP) electrospun mats. (c) ^{1}H NMR spectra of the P(VDF-HFP), and sulfonic acid-grafted P(VDF-HFP) with 1 and 15 wt % taurine feed contents in DMSO-d_6, respectively.

tensile samples were prepared according to the ASTM D638 standard. Each reported value was the average of at least five specimens.

The Brunauer–Emmett–Teller (BET) surface area of electrospun mats were measured using nitrogen gas physical adsorption method with a surface area analyzer. The porosity (P) of the electrospun mats were determined by the n-butanol uptake method. Typically, the dry membrane was immersed in n-butanol for 3 h, and the following equation was used to calculate the porosity:

$$P\ (\%) = \frac{M_{\mathrm{BuOH}}/\rho_{\mathrm{BuOH}}}{M_{\mathrm{BuOH}}/\rho_{\mathrm{BuOH}} + M_{\mathrm{m}}/\rho_{\mathrm{p}}} \quad (2)$$

M_{BuOH} is the mass of the absorbed n-butanol, M_{m} is the mass of dry membrane, and ρ_{BuOH} and ρ_{p} are the densities of n-butanol and the polymer, respectively.

The ionic conductivities were measured on an Autolab PGSTAT30 electrochemical workstation. IL-based polymer electrolytes were sandwiched between two polished stainless steel electrodes. AC impedances were determined over a frequency range of 10^5–10 Hz with AC amplitude of 10 mV. In complex plane graph, the intercept of high frequency curve with the horizontal axis was taken as the bulk resistance. Ionic conductivity (σ) of the electrolyte was calculated by eq 3

$$\sigma = \frac{L}{R \times S} \quad (3)$$

where L, R, and S are the thickness, the bulk resistance, and the area of the electrolyte, respectively. The impedance of each sample was measured five times to ensure data reproducibility. The electrolyte uptake and ionic conductivity were all measured at 20 °C and 50% relative humidity (RH).

Lithium transference numbers (T_{Li^+}) were measured using the method of chronoamperometry in the Li/electrolytes/Li cells with a polarization voltage of 30 mV (ΔV) according to our previous publication.[9] In brief, the initial current, I_0, and the steady-state current, I_{ss}, that flowed through the cell were measured. The same cell was also monitored by impedance spectroscopy in frequency range of 10^6–10^{-1} Hz to obtain the initial, R_0, and the steady-state, R_{ss}, Li/electrolyte resistance. The lithium transference numbers (T_{Li^+}) were given by eq 4

$$T_{\mathrm{Li}^+} = \frac{I_{\mathrm{ss}}(\Delta V - R_0 I_0)}{I_0(\Delta V - R_{\mathrm{ss}} I_{\mathrm{ss}})} \quad (4)$$

2.7. Fabrication and Testing of Electrochromic Device. PANI-TiO_2 emulsion in xylene was spin-coated onto cleaned ITO-coated glass to form thin film. Single-active-layer electrochromic devices with configuration of ITO glass/electrochromic layer (PANI-TiO_2)/electrolyte/ITO glass were fabricated. The visible transmittance spectra and switching kinetics of the devices were recorded on a UV–vis spectrophotometer (Shimadzu UV-2501 PC), by applying constant potentials and square-wave potentials using the Autolab PGSTAT 302 potentiostat/galvanostat analyzer, respectively. The switching kinetics of the devices were determined at the wavelength of 650 nm (λ_{max}), at which maximum transmittance contrast was achieved under the constant potentials. For the dynamic switching, the potential was stepped between −2.0 and +2.0 V with step intervals of 40 s.[31]

2.8. Assembly and Testing of Lithium-Ion Battery Cathode. A standard CR2032 coin cell with lithium metal as counter electrode was used for testing the electrochemical properties of the cathode. The working electrode was prepared by spreading a mixture of $LiCoO_2$ (80 wt %), Super-P (10 wt %), and PVDF (10 wt %) dispersed in N-methyl pyrrolidone (NMP) onto an aluminum foil current collector.

DOI: 10.1021/acsami.5b04034
ACS Appl. Mater. Interfaces 2015, 7, 16548–16557

Table 1. Elemental Analysis Results for Sulfonic Acid-Grafted P(VDF-HFP) Samples with Different Taurine Feed Contents

taurine feed content[a] (wt %)	theoretical SO_3H content[b] (mmol g^{-1})	carbon (wt %)	hydrogen (wt %)	nitrogen (wt %)	sulfur (wt %)	measured SO_3H content (mmol g^{-1})
1	0.08	34.72	2.48	0.11	0.23	0.07
3	0.24	34.63	2.52	0.21	0.62	0.19
5	0.39	34.52	2.52	0.40	1.05	0.33
10	0.75	34.42	2.60	0.65	1.67	0.52
15	1.10	34.29	2.82	1.13	2.62	0.82

[a]Calculated by the ratio of the taurine feed weight to the feed weight of P(VDF-HFP). [b]Assuming 100% conversion.

IL-based electrolytes were prepared by soaking original P(VDF-HFP) electrospun mats and P(VDF-HFP) electrospun mats tethered with 5 and 15 wt % lithium sulfonate (feed content) in 0.3 mol kg^{-1} LiTFSI/$PYR_{14}^{+}TFSI^{-}$ for 24 h in an argon filled glovebox. The electrochemical tests were performed on a NEWARE-CT3008 battery test system (Neware Technology Limited, Shenzhen, China). The cells were cycled between 2.8−4.2 V versus Li^{+}/Li.

3. RESULTS AND DISCUSSION

3.1. Sulfonic Acid-Grafted P(VDF-HFP) Electrospun Mats as Ionic Liquid Host. *3.1.1. Structures and Morphologies of the Sulfonic Acid-Grafted P(VDF-HFP) Electrospun Mats.* In this work, sulfonic acid is grafted onto P(VDF-HFP) polymer chains via a chemical route rather than electron beam radiation. As illustrated in Figure 1a, the grafting reaction is accompanied by the elimination of HF (dehydrofluorination) from VDF segments adjacent to HFP in the main chain to create C═N double bond.[29] The reaction is verified by FTIR and ^{1}H NMR studies. Figure 1b shows the FTIR spectra of P(VDF-HFP) and sulfonic acid-grafted P(VDF-HFP) electrospun mats. Compared with the spectra of neat P(VDF-HFP), an absorption band corresponding to the stretching vibration of C═N is observed at 1650 cm^{-1} for the sulfonic acid-grafted P(VDF-HFP). In addition, the characteristic peak at 1040 cm^{-1} belonging to the symmetric stretching vibration of O═S═O can also be clearly identified. Figure 1c shows the ^{1}H NMR spectra of P(VDF-HFP) and sulfonic acid-grafted P(VDF-HFP) with high and low feed contents of taurine. The new resonance at 8.1 ppm for sulfonic acid-grafted P(VDF-HFP) can be assigned to the hydroxyl proton of the sulfonic acid group,[32] and its intensity clearly increases with the feed content of taurine. The above results indicate that taurine has been successfully attached onto P(VDF-HFP) chains through dehydrofluorination of P(VDF-HFP) and the formation of C═N double bond.

Elementary analysis was conducted to quantify the sulfonic acid contents of the grafted P(VDF-HFP) samples. The sulfonic acid contents were calculated from the measured C/S atomic ratios. Table 1 shows the theoretical SO_3H contents (assuming 100% conversion) and the measured SO_3H contents of the sulfonic acid-grafted P(VDF-HFP) samples with different taurine feed contents. As can be observed, the grafted sulfonic acid content increases from 0.07 mmol g^{-1} for the sample with 1 wt % taurine feed content to 0.82 mmol g^{-1} for the sample with 15 wt % taurine feed content.

TGA was performed to investigate the thermal stabilities of the electrospun mats in air. Figure 2 shows the thermograms of the P(VDF-HFP) electrospun mats grafted with different amounts of sulfonic acid groups. Without grafting, the P(VDF-HFP) electrospun mats are thermally stable up to 400 °C. As expected, all the grafted electrospun mats exhibit poorer thermal stability than the corresponding neat copolymer owing to the presence of imine bonds (C═N). The decomposition

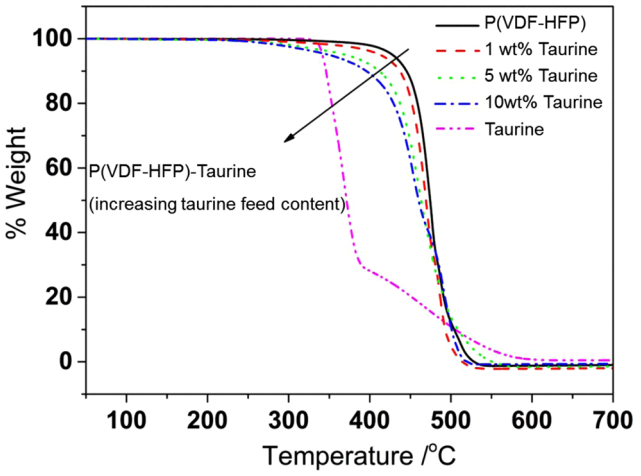

Figure 2. TGA curves of original P(VDF-HFP) electrospun mat and sulfonic acid-grafted P(VDF-HFP) electrospun mats at different taurine feed contents.

temperature, which is defined as the temperature at 5% weight loss, decreases with increasing the taurine feed content. Nevertheless, all the grafted electrospun mats are thermally stable up to 200 °C, which satisfies the safety requirement for most electrochemical devices.

To investigate the morphology of the sulfonic acid-grafted P(VDF-HFP) electrospun mats, SEM studies were conducted. Figure 3 shows SEM images and distributions of the nanofiber diameters of the sulfonic acid-grafted P(VDF-HFP) electrospun mats with different taurine feed contents. As can be observed, uniform bead-free nanofibers are obtained in the whole taurine content range studied. In addition, as the taurine content increases, the average fiber diameter decreases. For the taurine feed contents of 1, 5, and 10 wt %, the average fiber diameters are 110, 94, and 55 nm, respectively, which are much smaller than that of the neat P(VDF-HFP) nanofibers (128 nm). More SEM images and fiber diameter distributions taken for the electrospun P(VDF-HFP) mats with different taurine feed contents are provided in Figure S1 in the Supporting Information. The reduced fiber diameter can be attributed to the increase in the charge density of the polymer solutions because of the grafting of sulfonic acid. The excess ionic charges on the jets tend to elongate the jet, increasing the surface area and rendering the fibers smaller diameters.[33,34] In addition, merging and branching fibers can also be observed in Figure 3, which may influence mechanical properties of the electrospun mats, and will be discussed later.

Electrospun mats with thinner nanofibers typically exhibit higher porosity, that is, higher fraction of pore volume over the total volume of the mats, and larger specific surface area.[35] Table 2 summarizes the porosity and specific surface area values of the electrospun mats with various taurine feed contents.

DOI: 10.1021/acsami.5b04034
ACS Appl. Mater. Interfaces 2015, 7, 16548−16557

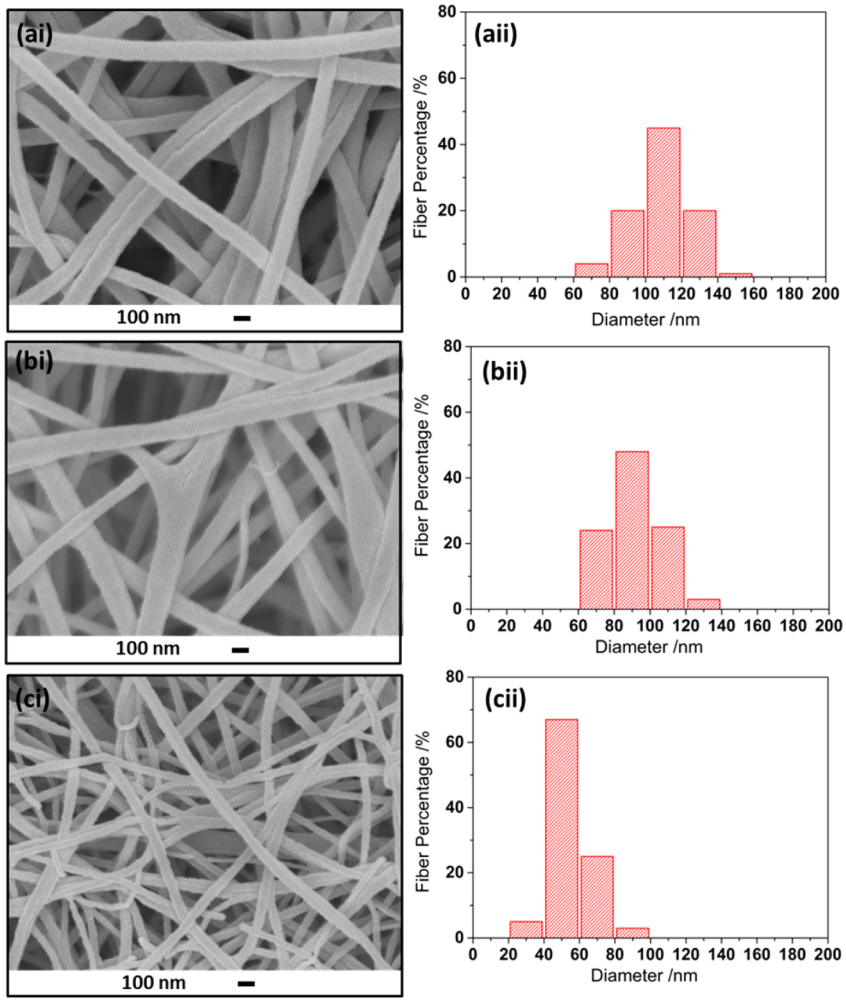

Figure 3. SEM images and histograms of fiber diameter distributions of sulfonic acid-grafted P(VDF-HFP) electrospun mats with (ai, aii) 1 wt %, (bi, bii) 5 wt %, and (ci, cii) 10 wt % taurine feed contents.

Table 2. Average Fiber Diameter, Porosity, and Specific Surface Area of Sulfonic Acid-Grafted P(VDF-HFP) Electrospun Mats with Different Taurine Feed Contents

	taurine feed contents		
properties	1 wt %	5 wt %	10 wt %
average fiber diameter (nm)	110	94	55
porosity (%)	83	85	89
specific surface area (m^2 g^{-1})	3.3	8.0	12.1

Obviously, both porosity and specific surface area increase with decreasing fiber diameter. The electrospun mat with 10 wt % taurine (feed content) exhibits the highest porosity of 89%, and the largest specific surface area of 12.1 m^2 g^{-1}. The high porosity facilitates the electrolyte uptake, while the large specific surface area promotes the interactions of the nanofibers with the liquid electrolyte in the pores, both of which will benefit ion transport properties of the resultant electrolytes.

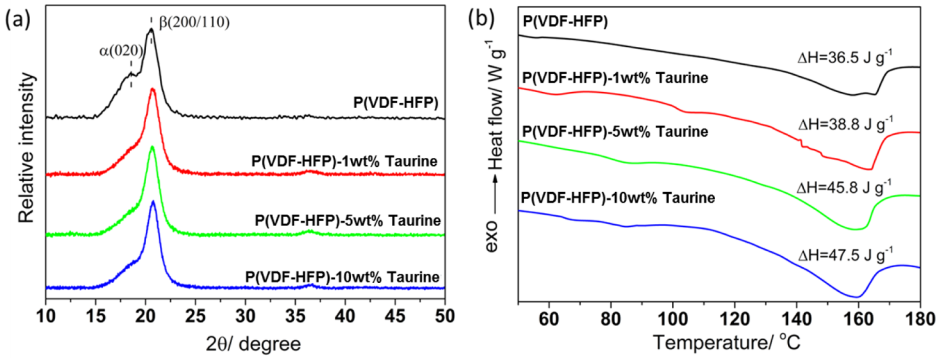

Figure 4. (a) WAXD patterns and (b) DSC thermograms of P(VDF-HFP) and sulfonic acid-grafted P(VDF-HFP) electrospun mats with different taurine feed contents.

DOI: 10.1021/acsami.5b04034
ACS Appl. Mater. Interfaces 2015, 7, 16548−16557

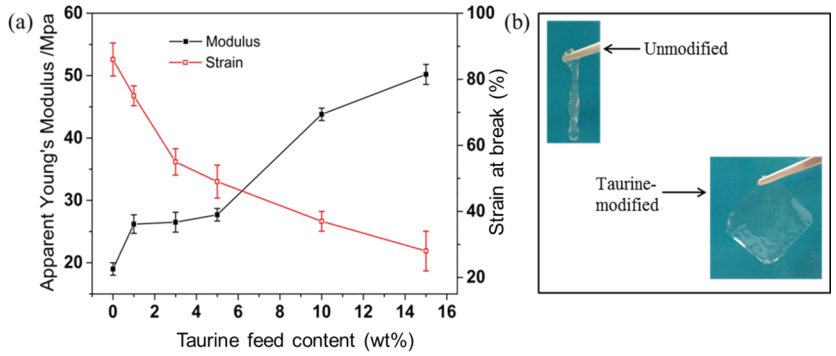

Figure 5. (a) Apparent Young's Modulus and strain at break of sulfonic acid-grafted P(VDF-HFP) electrospun mats with different taurine feed contents. (b) Picture showing the neat P(VDF-HFP) and sulfonic acid-grafted P(VDF-HFP) electrospun mat with 15 wt % taurine feed content after loading with the $BMIM^+BF_4^-$.

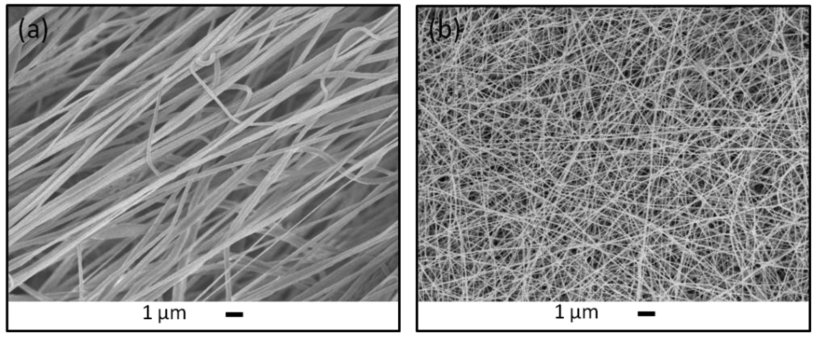

Figure 6. SEM images of (a) neat P(VDF-HFP) and (b) sulfonic acid-grafted P(VDF-HFP) electrospun mat with 15 wt % taurine feed content after stretching to break.

It has been demonstrated that the polar β phase and crystallinity for the P(VDF-HFP) electrospun mats are closely related to the orientation and stretching of the chains along the fiber axis as a result of the forces exerted in electrospinning process.[36] Thus, the incorporation of taurine, a charged chemical, is expected to induce a higher content of β phase and higher crystallinity owing to the improved chain orientation. As seen from Figure 4a, the intensity ratio of α (020) to β (200/110) diffraction peak decreases with the incorporation of taurine, indicating that the inclusion of taurine promotes the β phase that has all trans-conformation. The increase of the β-phase content in the electrospun mats is also verified by FTIR spectroscopy (Figure 1b). It is obvious that the intensities of the absorption bands at 840 and 1278 cm^{-1}, which are associated with the β phase of P(VDF-HFP), increase with the attachment of taurine. Figure 4b shows the typical DSC thermograms of the electrospun P(VDF-HFP) mats with different taurine feed contents. It shows that the enthalpy of fusion increases from 36.5 J g^{-1} for the neat P(VDF-HFP) electrospun mat to 47.5 J g^{-1} for the electrospun mat with 10 wt % taurine (feed content), indicating an increase of crystallinity after attaching taurine. The degree of crystallinity is about 44%, 47%, 55%, and 57%, respectively, for the P(VDF-HFP) electrospun mats with 0, 1, 5, and 10 wt % taurine (feed content). The data of XRD, FTIR, and DSC all support that the smaller diameters of the sulfonic acid-grafted electrospun nanofibers is mainly due to the charged nature of taurine, which elongates the jet, enhancing the chain orientation.

3.1.2. Mechanical Properties of the Sulfonic Acid-Grafted P(VDF-HFP) Electrospun Mats. For some electrochemical devices, such as lithium-ion batteries, the electrolytes must be able to withstand the pressure applied during device packaging and cycling. It is therefore of paramount importance to investigate mechanical properties of the electrospun mats and the IL-loaded mats. The apparent Young's Modulus and strain at break of the sulfonic acid-grafted P(VDF-HFP) electrospun mats with different taurine feed contents are shown in Figure 5a. All electrospun mats exhibit similar deformation behavior, as shown by the typical tensile curves in Figure S2 in the Supporting Information. The apparent Young's Modulus of the electrospun mats increases with the taurine feed content. The highest apparent Young's modulus of 50.2 MPa is obtained for electrospun mat with 15 wt % taurine (feed content), which is 164% higher than that of the neat P(VDF-HFP) mat. In addition, the strain at break of the electrospun mats shows a decreasing trend with increasing taurine content. The attachment of taurine induces the formation of β phase and increases the crystallinity of electrospun mats, both may lead to enhanced stiffness of the nanofibers. However, neither crystalline form nor crystallinity varies much with the taurine content. Therefore, the increase in apparent Young's Modulus is mainly due to the interconnected network structure formed by the branching and merging of the nanofibers. Figure 6 shows SEM images of the neat P(VDF-HFP) and sulfonic acid-grafted P(VDF-HFP) mats with 15 wt % taurine (feed content) after stretching to break. The alignment of fibers is observed for the neat P(VDF-HFP) mat, which is the likely reason for its large elongation at break, while for the electrospun mat with taurine, the random arrangement of the nanofibers retains. The result suggests that the merging and branching of the nanofibers help to improve the dimensional stability of the mats. In order to examine the effects of the IL on the structural integrity of the

DOI: 10.1021/acsami.5b04034
ACS Appl. Mater. Interfaces 2015, 7, 16548−16557

mat, the electrospun mats are immersed in $BMIM^+BF_4^-$. As shown in Figure 5b, a gel mass is formed for the IL-loaded neat P(VDF-HFP) mat. By contrast, a free-standing film is obtained for the IL-loaded sulfonic acid-grafted P(VDF-HFP) electrospun mats, which can be easily handled in device fabrication.

3.1.3. Effect of the Grafted Sulfonic Acid Groups on Ionic Conductivity. Electrolytes with ionic conductivity levels approaching or higher than 1 mS cm^{-1} is considered as a fundamental requirement for a variety of electrochemical devices.[37] Figure 7 shows ionic conductivity and electrolyte

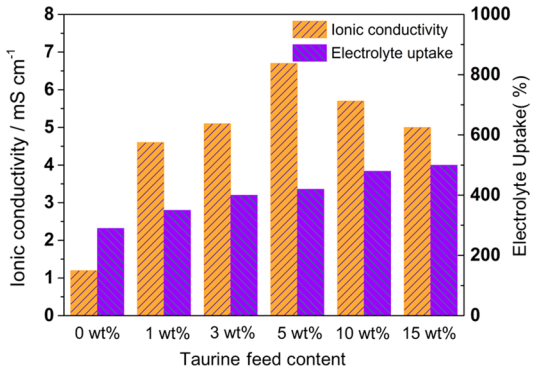

Figure 7. Ionic conductivity and electrolyte uptake of sulfonic acid-grafted P(VDF-HFP) electrospun mats with different taurine feed contents.

uptake of sulfonic acid-grafted P(VDF-HFP) electrospun mats with different taurine feed contents. The electrolyte uptake, which is due to the swelling of the polymer matrix and filling the pores of the electrospun mats, increases monotonically with the taurine feed content. This is mainly due to the increased porosity and specific surface area caused by the decreased fiber diameter, which help to trap more IL in the pores. It is worth noting that in IL-loaded electrospun mats, the liquid phase should have the highest ionic conductivity and be the major contributor to the overall conductivity. Thus, the increased IL content in the pores can significantly improve the ionic conductivity. As shown in Figure 7, ionic conductivity increases with taurine feed content up to 5 wt %, followed by a slight drop. The highest ionic conductivity of 6.7 mS cm^{-1} is achieved at 5 wt % taurine feed content, which is even higher than the conductivity of neat $BMIM^+BF_4^-$ (3.5 mS cm^{-1}).[38] This is likely due to the Lewis acid−base interaction between the grafted SO_3^- groups and $BMIM^+$ of ILs, which promotes the dissociation of ILs and releases more free ions. In addition to the effect arising from the increased number of free ions from IL, the sulfonic acid groups can also function as proton conduction sources, providing some small conduction ions. It is believed that the increased amounts of free ions from the IL should contribute more to the overall increase in ionic conductivity, considering that the amount of grafted sulfonic acid groups is much lower than the amount of the IL in the system. Consequently, the significantly improved ionic conductivity is ascribed to the increased IL uptake combined with the favorable interactions of the grafted SO_3^- groups with $BMIM^+$ of ILs, which promotes the dissociation of ILs, as well as the additional proton conduction. The increase in ionic conductivity is more pronounced for the mat with 5 wt % taurine feed content than those with 10 and 15 wt % taurine feed contents despite the later ones have higher IL contents. This may be attributed to the possibility of formation of hydrogen bonds among sulfonic acid groups at higher sulfonic acid contents, which may impede their interactions with ILs.

To verify the interactions between the grafted sulfonic acid groups and cations ($BMIM^+$) of IL, FTIR measurement was performed. P(VDF-HFP)-taurine/$BMIM^+BF_4^-$ film with 5 wt % IL prepared by solution casting (in DMF) was used in the test. In Figure 8, the band at 1040 cm^{-1} in the neat P(VDF-

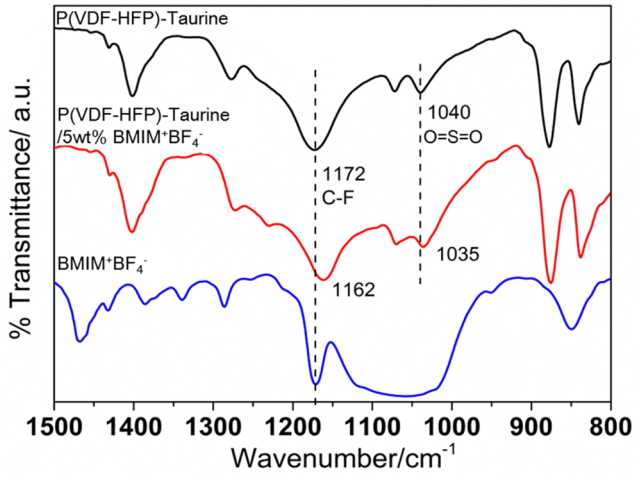

Figure 8. FTIR spectra of P(VDF-HFP)-taurine, $BMIM^+BF_4^-$, and P(VDF-HFP)-taurine/$BMIM^+BF_4^-$ solution cast film with 5 wt % $BMIM^+BF_4^-$.

HFP)-taurine is ascribed to the symmetric stretching vibration of O═S═O. This band shifts to 1035 cm^{-1} after loading with IL, which can be attributed to the Lewis acid−base interactions between the SO_3^- groups and cations of the IL.[39] This positive interaction promotes the dissociation of ILs, meanwhile provides additional protons, resulting in improved ionic conductivity. Besides, C−F stretching vibration peak at 1172 cm^{-1} also shifts to 1162 cm^{-1} after loading IL, which is presumably caused by the complexation of the polymer backbone with the IL.[40,41]

3.2. IL-Loaded Sulfonic Acid-Grafted P(VDF-HFP) Electrospun Mats As Electrolytes in Electrochromic Devices. Electrochromic devices are able to reversibly change their light absorption properties in a certain wavelength range via redox reactions upon the application of external potentials and have found applications in a wide range of areas, such as smart windows and displays. Electrolytes in electrochromic devices play an important role in influencing their electrochromic performance. IL-based electrolytes have been demonstrated suitable for the use in electrochromic devices due to their superiority in safety compared with traditional gel electrolytes.[19,42−44] Since the device performance is highly dependent on the doping and dedoping process of the electrochromic layer, it is beneficial to introduce smaller ions. Polyaniline (PANI) is the most widely studied π-conjugated polymers for electrochromic devices. In comparison with transition metal oxides, PANI in general requires lower switching potential and displays higher optical contrast as well as faster response speed.[45] We hypothesized that the grafted sulfonic acid groups would provide additional proton conduction, therefore facilitate the injection and extraction of cations into/from PANI and improve the device performance. Sulfonate anions could also interact with PANI chains when they are in radical cation states,[46] improving the interactions

DOI: 10.1021/acsami.5b04034
ACS Appl. Mater. Interfaces 2015, 7, 16548−16557

between the electrochromic layer and electrolyte. Herein, we demonstrate that by using this novel proton conducting IL-based electrolyte, PANI-based electrochromic device exhibits higher transmittance contrast and much faster switching speed. In order to investigate the effects of proton conductivity on the device performance more clearly, the electrospun mats with the highest taurine feed content (15 wt %) is used as the ionic liquid host. Figure 9 shows the switching behaviors of the

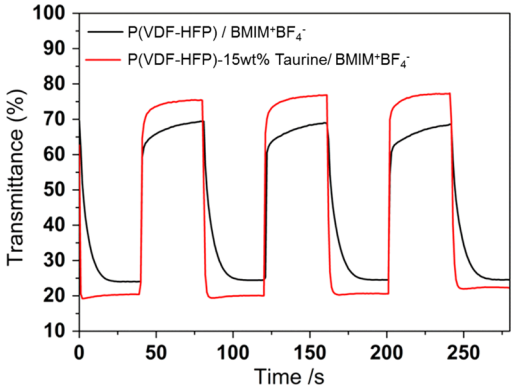

Figure 9. Switching curves of the electrochromic devices with P(VDF-HFP)/$BMIM^+BF_4^-$ and P(VDF-HFP)-15 wt % taurine (feed content)/$BMIM^+BF_4^-$ as electrolytes under square-wave potentials oscillating between +2.0 and −2.0 V.

devices under the applied step potential between +2.0 V and −2.0 V at the wavelength of 650 nm (λ_{max}). The maximum changes in transmittance (ΔT) obtained from Figure 9 are compared in Table 3. The coloration time and bleaching time,

Table 3. Electrochromic Properties of the Devices Using P(VDF-HFP)/$BMIM^+BF_4^-$ and P(VDF-HFP)−15 wt % taurine (feed content)/$BMIM^+BF_4^-$ as electrolytes, respectively

electrolyte	ΔT (%)	coloration time (s)	bleaching time (s)
P(VDF-HFP)/$BMIM^+BF_4^-$	45	11.0	7.2
P(VDF-HFP)−15 wt % taurine/ $BMIM^+BF_4^-$	56.2	2.0	2.5

which are defined as the periods required for the device switching to its 90% and 10% of its maximum transmittance contrast, respectively, are also listed in Table 3. The device with P(VDF-HFP)-15 wt % Taurine (feed content)/$BMIM^+BF_4^-$ electrolyte shows higher transmittance contrast of (ΔT = 56%), shorter coloration time (2.0 s) and bleaching time (2.5 s) than the device with P(VDF-HFP)/$BMIM^+BF_4^-$. It indicates that protons can easily diffuse into the electrochromic layer, allowing more active units be switched and faster switching of the devices.

3.3. IL-Loaded Lithium Sulfonate-Grafted P(VDF-HFP) Electrospun Mats as Electrolytes in Lithium-Ion Batteries. The potential of ILs as electrolytes for energy storage devices, including lithium-ion batteries, has long been appreciated. Despite the unique advantages of IL-based electrolytes, such as nonflammability, nonvolatility and excellent electrochemical stability, their rather low Li^+ ion conductivity may deteriorate the device performance under high current density owing to the ion concentration gradients created in the cell. Tethering Li^+ counterions onto P(VDF-HFP) electrospun mats offers a possible route to provide additional Li^+ conductions and increase the lithium transference numbers (T_{Li^+}) of the electrolytes. Thus, lithium sulfonate-grafted P(VDF-HFP) was prepared using a similar method as that of sodium sulfonate-grafted P(VDF-HFP). Again, FTIR was used to characterize the chemical structure of lithium sulfonate-grafted P(VDF-HFP). The symmetric stretching vibration of O═S═O group appears at 1043 cm^{-1} in the FTIR spectrum of lithium sulfonate-grafted P(VDF-HFP) (Figure S3 in the Supporting Information) and it shows a shift (3 cm^{-1}) compared with that of sulfonic acid-grafted P(VDF-HFP), indicating the successful displacement reaction. Figure S4 in the Supporting Information shows SEM images and distributions of the nanofiber diameters of the lithium sulfonate-grafted P(VDF-HFP) electrospun mats. Compared with the sulfonic acid-grafted P(VDF-HFP) electrospun mats, the average fiber diameter of the lithium sulfonate-grafted P(VDF-HFP) mats further decreases to 50 and 40 nm, respectively, for electrospun mats with 5 and 15 wt % lithium sulfonate (feed contents). The reduced fiber diameter is ascribed to the increased charge density of the solutions used in electrospinning due to the conversion of sulfonic acid to lithium sulfonate.

To demonstrate the effectiveness of the lithium sulfonate-grafted P(VDF-HFP) electrospun mats in improving Li^+ transport properties, three IL hosts were evaluated, namely neat P(VDF-HFP) mats, P(VDF-HFP) mats modified with 5 and 15 wt % lithium sulfonate (feed content), respectively, which were all loaded with 0.3 mol kg^{-1} LiTFSI/$PYR_{14}^+TFSI^-$. Their T_{Li^+} values were measured using DC polarization method combined with impedance techniques, as shown in Figure S5 in the Supporting Information, and calculated using eq 4. The measured T_{Li^+} values of neat P(VDF-HFP) mats, P(VDF-HFP) electrospun mats with 5 and 15 wt % lithium sulfonate (feed content) are 0.24, 0.28, and 0.52, respectively. The higher T_{Li+} value for lithium sulfonate-grafted P(VDF-HFP) electrospun mats suggests that the mobile Li^+ ions coupled to polymer chains could hop between immobilized SO_3^- anions, allowing a relatively fast movement of the Li^+ ion and hence leading to improved T_{Li^+} value. A high T_{Li^+} would decrease the electrolyte polarization caused by anion accumulation and suppress the concentration gradient to facilitate lithium-ion transport, which is beneficial for the rate performance of lithium-ion batteries. Figure 10 shows the discharge C-rate capabilities of the Li/$LiCoO_2$ cells containing the aforementioned three electrolyte systems. All the cells exhibit similar capacities of about 120 mAh g^{-1} at 0.1 C. Their performance difference, however, becomes prominent at higher current densities where the influence of lithium-ion conductivity is more crucial. It is clear that P(VDF-HFP) electrospun mat modified with 15 wt % lithium sulfonate (feed content) exhibits the highest discharge capacity at each C-rate, and its performance becomes outstanding when the current density is 0.6 C or higher. Obviously, the remarkable improvement in the rate performance of Li-ion battery is due to the enhanced lithium-ion conductivity provided by the lithium sulfonate-grafted P(VDF-HFP) nanofibrous mats.

4. CONCLUSIONS

In summary, the P(VDF-HFP) copolymer is successfully functionalized with sulfonic acid through the attachment of taurine. FESEM studies show that the P(VDF-HFP) copolymer with higher sulfonic acid contents can produce thinner fibers by

DOI: 10.1021/acsami.5b04034
ACS Appl. Mater. Interfaces 2015, 7, 16548−16557

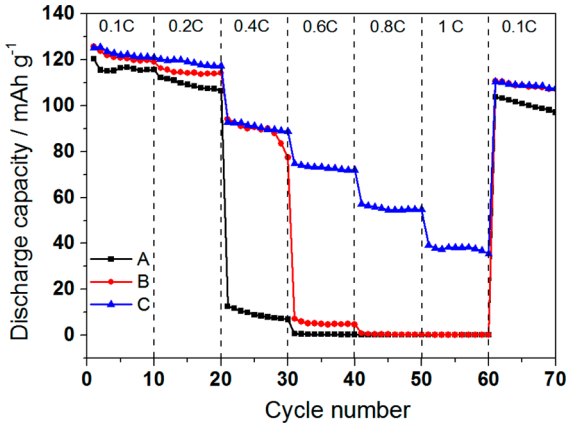

Figure 10. Rate discharge capacity of Li/$LiCoO_2$ cells under different current density (A, B and C represent neat P(VDF-HFP) electrospun mats, P(VDF-HFP) electrospun mats with 5 and 15 wt % lithium sulfonate (feed content), respectively, after loading with 0.3 mol kg^{-1} LiTFSI/$PYR_{14}{}^{+}TFSI^{-}$).

electrospinning, while there are interfiber junctions at all sulfonic acid contents, leading to remarkable improvement in dimensional stability of the electrospun mats. Free-standing IL-loaded electrolytes can be facilely prepared by immersing the electrospun sulfonic acid-grafted P(VDF-HFP) mats in the IL. Significant enhancement of ionic conductivity is observed with the attached taurine, which can be attributed to the greater extents of dissociation of the IL and additional proton conduction owing to the Lewis acid−base interactions between the SO_3^- groups and cations of IL. The electrochromic device with the IL-loaded P(VDF-HFP)−15 wt % taurine (feed content) electrolyte exhibits higher contrast (56%), shorter coloration (2.0 s) and bleaching time (2.5 s) than that with P(VDF-HFP)/$BMIM^{+}BF_4^-$ electrolyte. The enhanced device performance can be ascribed to the easy diffusion of protons into the electrochromic layer, allowing more active units be switched and faster switching of the device. Furthermore, the sulfonic acid-grafted P(VDF-HFP) electrospun mat can be lithiated. Mobile Li^+ ions provided by the lithium sulfonate-grafted P(VDF-HFP) polymer chains can provide additional lithium-ion conduction to the IL-based electrolyte, with which Li/$LiCoO_2$ batteries display enhanced C-rate performance. This demonstrated the potential of the lithium sulfonate-grafted P(VDF-HFP) electrospun mats for high-performance solvent-free lithium-ion batteries.

■ ASSOCIATED CONTENT

Supporting Information

SEM images and histograms of fiber diameter distributions of sulfonic acid-grafted P(VDF-HFP) electrospun mats with different taurine feed contents; Apparent stress−strain curves of the P(VDF-HFP) electrospun mats with different taurine feed contents; FTIR spectra of P(VDF-HFP), sulfonic acid-grafted P(VDF-HFP), and lithium sulfonate-grafted P(VDF-HFP) electrospun mats; SEM images and histograms of fiber diameter distributions of lithium sulfonate-grafted P(VDF-HFP) electrospun mats; Chronoamperometric curves of Li/electrolyte/Li symmetric cells with original P(VDF-HFP) electrospun mats, and P(VDF-HFP) electrospun mats tethered with 5 and 15 wt % lithium sulfonate (feed content) loaded with 0.3 mol kg^{-1} LiTFSI/$PYR_{14}{}^{+}TFSI^{-}$ as electrolytes. The Supporting Information is available free of charge on the ACS Publications website at DOI: 10.1021/acsami.5b04034.

■ AUTHOR INFORMATION

Corresponding Author

*E-mail: asxhlu@ntu.edu.sg.

Notes

The authors declare no competing financial interest.

■ ACKNOWLEDGMENTS

R.Z. thanks Nanyang Technological University, Singapore, for providing her Ph.D. scholarship in course of this work. This work was supported by Science and Engineering Research Council of the Agency for Science, Technology and Research (A*Star) and Ministry of National Development, Singapore under Grants 132 176 0013 and 132 176 0011.

■ REFERENCES

(1) Oh, K.-H.; Lee, D.; Choo, M.-J.; Park, K. H.; Jeon, S.; Hong, S. H.; Park, J.-K.; Choi, J. W. Enhanced Durability of Polymer Electrolyte Membrane Fuel Cells by Functionalized 2d Boron Nitride Nanoflakes. *ACS Appl. Mater. Interfaces* **2014**, *6*, 7751−7758.

(2) Zhou, R.; Liu, W. S.; Kong, J. H.; Zhou, D.; Ding, G. Q.; Leong, Y. W.; Pallathadka, P. K.; Lu, X. H. Chemically Cross-Linked Ultrathin Electrospun Poly(Vinylidene Fluoride-Co-Hexafluoropropylene) Nanofibrous Mats as Ionic Liquid Host in Electrochromic Devices. *Polymer* **2014**, *55*, 1520−1526.

(3) Wang, S. H.; Kuo, P. L.; Hsieh, C. T.; Teng, H. Design of Poly(Acrylonitrile)-Based Gel Electrolytes for High-Performance Lithium Ion Batteries. *ACS Appl. Mater. Interfaces* **2014**, *6*, 19360−19370.

(4) Elabd, Y. A.; Hickner, M. A. Block Copolymers for Fuel Cells. *Macromolecules* **2011**, *44*, 1−11.

(5) Moon, W. G.; Kim, G.-P.; Lee, M.; Song, H. D.; Yi, J. A Biodegradable Gel Electrolyte for Use in High-Performance Flexible Supercapacitors. *ACS Appl. Mater. Interfaces* **2015**, *7*, 3503−3511.

(6) Wilken, S.; Xiong, S.; Scheers, J.; Jacobsson, P.; Johansson, P. Ionic Liquids in Lithium Battery Electrolytes: Composition Versus Safety and Physical Properties. *J. Power Sources* **2015**, *275*, 935−942.

(7) Xie, Z.-L.; Huang, X.; Taubert, A. Dyeionogels: Proton-Responsive Ionogels Based on a Dye-Ionic Liquid Exhibiting Reversible Color Change. *Adv. Funct. Mater.* **2014**, *24*, 2837−2843.

(8) McDanel, W. M.; Cowan, M. G.; Carlisle, T. K.; Swanson, A. K.; Noble, R. D.; Gin, D. L. Cross-Linked Ionic Resins and Gels from Epoxide-Functionalized Imidazolium Ionic Liquid Monomers. *Polymer* **2014**, *55*, 3305−3313.

(9) Zhou, R.; Pramoda, K. P.; Liu, W.; Zhou, D.; Ding, G.; He, C.; Leong, Y. W.; Lu, X. Electrospun Poly(Vinylidene Fluoride) Copolymer/Octahydroxy-Polyhedral Oligomeric Silsesquioxane Nanofibrous Mats as Ionic Liquid Host: Enhanced Salt Dissociation and Its Function in Electrochromic Device. *Electrochim. Acta* **2014**, *146*, 224−230.

(10) Delahaye, E.; Goebel, R.; Loebbicke, R.; Guillot, R.; Sieber, C.; Taubert, A. Silica Ionogels for Proton Transport. *J. Mater. Chem.* **2012**, *22*, 17140−17146.

(11) Horowitz, A. I.; Panzer, M. J. High-Performance, Mechanically Compliant Silica-Based Ionogels for Electrical Energy Storage Applications. *J. Mater. Chem.* **2012**, *22*, 16534−16539.

(12) Herath, M. B.; Hickman, T.; Creager, S. E.; DesMarteau, D. D. A New Fluorinated Anion for Room-Temperature Ionic Liquids. *J. Fluorine Chem.* **2011**, *132*, 52−56.

(13) Visentin, A. F.; Panzer, M. J. Poly(Ethylene Glycol) Diacrylate-Supported Lonogels with Consistent Capacitive Behavior and Tunable Elastic Response. *ACS Appl. Mater. Interfaces* **2012**, *4*, 2836−2839.

(14) Zapata, P.; Mountz, D.; Meredith, J. C. High-Throughput Characterization of Novel Pvdf/Acrylic Polyelectrolyte Semi-Inter-

DOI: 10.1021/acsami.5b04034
ACS Appl. Mater. Interfaces 2015, 7, 16548−16557

penetrated Network Proton Exchange Membranes. *Macromolecules* **2010**, *43*, 7625−7636.
(15) Yee, W. A.; Xiong, S.; Ding, G.; Nguyen, C. A.; Lee, P. S.; Ma, J.; Kotaki, M.; Liu, Y.; Lu, X. Supercritical Carbon Dioxide-Treated Electrospun Poly(Vinylidene Fluoride) Nanofibrous Membranes: Morphology, Structures and Properties as an Ionic-Liquid Host. *Macromol. Rapid Commun.* **2010**, *31*, 1779−1784.
(16) Kim, J.-K.; Niedzicki, L.; Scheers, J.; Shin, C.-R.; Lim, D.-H.; Wieczorek, W.; Johansson, P.; Ahn, J.-H.; Matic, A.; Jacobsson, P. Characterization of N-Butyl-N-Methyl-Pyrrolidinium Bis-(Trifluoromethanesulfonyl)Imide-Based Polymer Electrolytes for High Safety Lithium Batteries. *J. Power Sources* **2013**, *224*, 93−98.
(17) Verma, R.; Tomar, N.; Creager, S. E.; Smith, D. W. Statically Non-Wetting Electrospun Perfluorocyclobutyl (Pfcb) Aryl Ether Polymer Doped with Room Temperature Ionic Liquid (Rtil). *Polymer* **2012**, *53*, 2211−2216.
(18) Zhou, D.; Zhou, R.; Chen, C.; Yee, W. A.; Kong, J.; Ding, G.; Lu, X. Non-Volatile Polymer Electrolyte Based on Poly(Propylene Carbonate), Ionic Liquid, and Lithium Perchlorate for Electrochromic Devices. *J. Phys. Chem. B* **2013**, *117*, 7783−7789.
(19) Desai, S.; Shepherd, R. L.; Innis, P. C.; Murphy, P.; Hall, C.; Fabretto, R.; Wallace, G. G. Gel Electrolytes with Ionic Liquid Plasticiser for Electrochromic Devices. *Electrochim. Acta* **2011**, *56*, 4408−4413.
(20) Marczewski, M. J.; Stanje, B.; Hanzu, I.; Wilkening, M.; Johansson, P. "Ionic Liquids-in-Salt" - a Promising Electrolyte Concept for High-Temperature Lithium Batteries? *Phys. Chem. Chem. Phys.* **2014**, *16*, 12341−12349.
(21) Tsuzuki, S.; Hayamizu, K.; Seki, S. Origin of the Low-Viscosity of Emim (Fso2)(2)N Ionic Liquid and Its Lithium Salt Mixture: Experimental and Theoretical Study of Self-Diffusion Coefficients, Conductivities, and Intermolecular Interactions. *J. Phys. Chem. B* **2010**, *114*, 16329−16336.
(22) Zhou, Q.; Boyle, P. D.; Malpezzi, L.; Mele, A.; Shin, J.-H.; Passerini, S.; Henderson, W. A. Phase Behavior of Ionic Liquid−Lix Mixtures: Pyrrolidinium Cations and Tfsi−Anions − Linking Structure to Transport Properties. *Chem. Mater.* **2011**, *23*, 4331−4337.
(23) Paronen, M.; Sundholm, F.; Ostrovskii, D.; Jacobsson, P.; Jeschke, G.; Rauhala, E.; Tikkanen, P. Preparation of Proton-Conducting Membranes by Direct Sulfonation. 1. Effect of Radicals and Radical Decay on the Sulfonation of Poly(Vinyl Fluoride) Films. *Chem. Mater.* **2003**, *15*, 4447−4455.
(24) Hietala, S.; Holmberg, S.; Karjalainen, M.; Nasman, J.; Paronen, M.; Serimaa, R.; Sundholm, F.; Vahvaselka, S. Structural Investigation of Radiation Grafted and Sulfonated Poly(Vinylidene Fluoride), Pvdf, Membranes. *J. Mater. Chem.* **1997**, *7*, 721−726.
(25) Yang, A. C. C.; Narimani, R.; Frisken, B. J.; Holdcroft, S. Investigations of Crystallinity and Chain Entanglement on Sorption and Conductivity of Proton Exchange Membranes. *J. Membr. Sci.* **2014**, *469*, 251−261.
(26) Ko, K. S.; Backus, R. C.; Berg, J. R.; Lame, M. W.; Rogers, Q. R. Differences in Taurine Synthesis Rate among Dogs Relate to Differences in Their Maintenance Energy Requirement. *J. Nutr.* **2007**, *137*, 1171−1175.
(27) Shin, Y. J.; Kang, S. J.; Jung, H. J.; Park, Y. J.; Bae, I.; Choi, D. H.; Park, C. Chemically Cross-Linked Thin Poly(Vinylidene Fluoride-Co-Trifluoroethylene)Films for Nonvolatile Ferroelectric Polymer Memory. *ACS Appl. Mater. Interfaces* **2011**, *3*, 582−589.
(28) Schmiegel, W. W. Crosslinking of Elastomeric Vinylidene Fluoride Copolymers with Nucleophiles. *Angew. Makromol. Chem.* **1979**, *76*−*7*, 39−65.
(29) Taguet, A.; Ameduri, B.; Dufresne, A. Crosslinking and Characterization of Commercially Available Poly(Vdf-Co-Hfp) Co-polymers with 2,4,4-Trimethyl-1,6-Hexanediamine. *Eur. Polym. J.* **2006**, *42*, 2549−2561.
(30) Xiong, S. X.; Phua, S. L.; Dunn, B. S.; Ma, J.; Lu, X. H. Covalently Bonded Polyaniline-Tio2 Hybrids: A Facile Approach to Highly Stable Anodic Electrochromic Materials with Low Oxidation Potentials. *Chem. Mater.* **2010**, *22*, 255−260.
(31) Xiong, S.; Jia, P.; Mya, K. Y.; Ma, J.; Boey, F.; Lu, X. Star-Like Polyaniline Prepared from Octa(Aminophenyl) Silsesquioxane: Enhanced Electrochromic Contrast and Electrochemical Stability. *Electrochim. Acta* **2008**, *53*, 3523−3530.
(32) Flach, A. M.; Johnson, F. E.; Cabasso, I. Synthesis and Characterization of Fluorinated Polyionomers. Part I: Polyperfluoro-Sulfonylethoxy Propylene Vinyl Ether Sulfonimides Containing Aryl Sulfonic Acids. *Polym. Chem.* **2013**, *4*, 3370−3383.
(33) Chen, H.; Snyder, J. D.; Elabd, Y. A. Electrospinning and Solution Properties of Nafion and Poly(Acrylic Acid). *Macromolecules* **2008**, *41*, 128−135.
(34) Li, D.; Xia, Y. N. Electrospinning of Nanofibers: Reinventing the Wheel? *Adv. Mater.* **2004**, *16*, 1151−1170.
(35) Pai, C. L.; Boyce, M. C.; Rutledge, G. C. On the Importance of Fiber Curvature to the Elastic Moduli of Electrospun Nonwoven Fiber Meshes. *Polymer* **2011**, *52*, 6126−6133.
(36) Liu, Y.-L.; Li, Y.; Xu, J.-T.; Fan, Z.-Q. Cooperative Effect of Electrospinning and Nanoclay on Formation of Polar Crystalline Phases in Poly(Vinylidene Fluoride). *ACS Appl. Mater. Interfaces* **2010**, *2*, 1759−1768.
(37) Dias, F. B.; Plomp, L.; Veldhuis, J. B. J. Trends in Polymer Electrolytes for Secondary Lithium Batteries. *J. Power Sources* **2000**, *88*, 169−191.
(38) Hanabusa, K.; Fukui, H.; Suzuki, M.; Shirai, H. Specialist Gelator for Ionic Liquids. *Langmuir* **2005**, *21*, 10383−10390.
(39) Yang, J. S.; Che, Q. T.; Zhou, L.; He, R. H.; Savinell, R. F. Studies of a High Temperature Proton Exchange Membrane Based on Incorporating an Ionic Liquid Cation 1-Butyl-3-Methylimidazolium into a Nafion Matrix. *Electrochim. Acta* **2011**, *56*, 5940−5946.
(40) Shalu; Chaurasia, S. K.; Singh, R. K.; Chandra, S. Thermal Stability, Complexing Behavior, and Ionic Transport of Polymeric Gel Membranes Based on Polymer Pvdf-Hfp and Ionic Liquid, Bmim Bf4. *J. Phys. Chem. B* **2013**, *117*, 897−906.
(41) Sim, L. N.; Majid, S. R.; Arof, A. K. Effects of 1-Butyl-3-Methyl Imidazolium Trifluoromethanesulfonate Ionic Liquid in Poly(Ethyl Methacrylate)/Poly(Vinylidenefluoride-Co-Hexafluoropropylene) Blend Based Polymer Electrolyte System. *Electrochim. Acta* **2014**, *123*, 190−197.
(42) Kavanagh, A.; Copperwhite, R.; Oubaha, M.; Owens, J.; McDonagh, C.; Diamond, D.; Byrne, R. Photo-Patternable Hybrid Ionogels for Electrochromic Applications. *J. Mater. Chem.* **2011**, *21*, 8687−8693.
(43) Kavanagh, A.; Fraser, K. J.; Byrne, R.; Diamond, D. An Electrochromic Ionic Liquid: Design, Characterization, and Performance in a Solid-State Platform. *ACS Appl. Mater. Interfaces* **2013**, *5*, 55−62.
(44) Oesterholm, A. M.; Shen, D. E.; Dyer, A. L.; Reynolds, J. R. Optimization of Pedot Films in Ionic Liquid Supercapacitors: Demonstration as a Power Source for Polymer Electrochromic Devices. *ACS Appl. Mater. Interfaces* **2013**, *5*, 13432−13440.
(45) Thakur, V. K.; Ding, G.; Ma, J.; Lee, P. S.; Lu, X. Hybrid Materials and Polymer Electrolytes for Electrochromic Device Applications. *Adv. Mater.* **2012**, *24*, 4071−4096.
(46) Jia, P.; Argun, A. A.; Xu, J.; Xiong, S.; Ma, J.; Hammond, P. T.; Lu, X. High-Contrast Electrochromic Thin Films Via Layer-by-Layer Assembly of Starlike and Sulfonated Polyaniline. *Chem. Mater.* **2010**, *22*, 6085−6091.

DOI: 10.1021/acsami.5b04034
ACS Appl. Mater. Interfaces 2015, 7, 16548−16557